IOP PUBLISHING JOURNAL OF PHYSICS D: APPLIED PHYSICS

J. Phys. D: Appl. Phys. **41** (2008) 094006 (12pp) doi:10.1088/0022-3727/41/9/094006

INVITED PAPER

New light from hybrid inorganic–organic emitters

C R Belton[1], G Itskos[2], G Heliotis[1], P N Stavrinou[1], P G Lagoudakis[3], J Lupton[3], S Pereira[4], E Gu[5], C Griffin[5], B Guilhabert[5], I M Watson[5], A R Mackintosh[6], R A Pethrick[6], J Feldmann[3], R Murray[1], M D Dawson[5] and D D C Bradley[1]

[1] The Blackett Laboratory, Imperial College London, Prince Consort Road, SW7 2AZ, London, UK
[2] Department of Physics, University of Cyprus, Nicosia, PO Box 20537, Cyprus
[3] Department of Physics, Ludwig-Maximilians-Universität, 80799 Munich, Germany
[4] CICECO, Departamento de Física, Universidade de Aveiro, 3810-193 Aveiro, Portugal
[5] Institute of Photonics, SUPA, University of Strathclyde, 106 Rottenrow, G4 0NW, Glasgow, UK
[6] Department of Pure and Applied Chemistry, University of Strathclyde, 295 Cathedral Street, Glasgow G1 1XL, UK

E-mail: c.belton@imperial.ac.uk and d.bradley@imperial.ac.uk

Received 23 October 2007, in final form 17 December 2007
Published 4 April 2008
Online at stacks.iop.org/JPhysD/41/094006

Abstract

We present the highlights of a research programme on hybrid inorganic–organic light emitters. These devices combine recent developments in III–V nitride technology (including UV emitting micro-arrays and specifically tailored quantum wells) with conjugated polymers to access the entire visible spectrum. Two types of devices are studied, those based on down conversion of the quantum well emission by radiative transfer and those based on non-radiative resonant energy transfer. The spectral and operating characteristics of the devices are described in detail. Selectable colour micro-arrays and bar emitters are demonstrated. The nature of the non-radiative energy transfer process has also been studied and we find transfer efficiencies of up to 43% at 15 K, with a $1/R^2$ dependence on the distance between quantum well and polymer layer, suggesting a plane–plane interaction. The relative importance of the non-radiative resonant energy transfer process increases with temperature to be up to 20 times more efficient, at 300 K, than the radiative transfer process.

(Some figures in this article are in colour only in the electronic version)

1. Introduction

Electrically generated light is one of the great advances of the modern world. However, with an increasing emphasis on more efficient and environmentally benign lighting systems as well as advancing interest in active light control for a variety of applications, it has become more important than ever to progress the development of new light sources. An important issue is the efficient generation of light with a distribution of photon energies that closely matches the characteristics of natural white light for energy efficient, solid-state lighting applications. In addition there is an increasing appetite for small-scale programmable light sources for use in micro-displays, imaging systems, miniature chemical and biological sensors and integrated lab-on-a-chip devices. In response to these needs, a research programme was initiated on hybrid light-emitting devices based on a synergistic combination of III-nitride and semi-conducting conjugated polymer technologies. The specific aim of this programme was to progress devices that possess a combination of the attractive electrical properties of inorganic materials and the high photoluminescence yields across the visible spectrum that are typical of organic materials [1].

1.1. Hybrids using radiative energy transfer

Using AlInGaN nitride materials, novel micro-structured light-emitting diodes (micro-LEDs) in various formats, including two-dimensional (2D) arrays of micro-discs and 1D arrays of

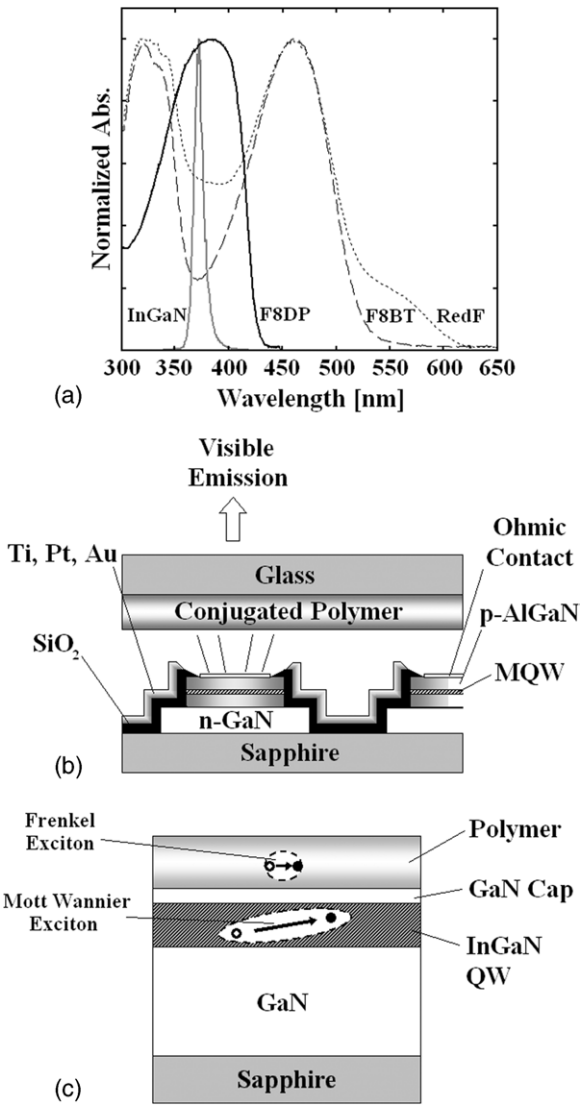

Figure 1. (*a*) Normalized absorption spectra of F8DP (——), F8BT (----) and Red F (· · · · · ·). Also shown is an emission spectrum typical of the InGaN structures used in this work (grey line). Note the overlap with F8DP absorption. (*b*) Device structure of a hybrid array element where a polymer layer is radiatively excited by a micro-LED (*c*) Schematic of a hybrid quantum well structure for FRET studies.

micro-stripes, have been successfully fabricated [2–8]. These micro-LED arrays consist of individual emitting elements of diameter/width typically ∼20 μm on a typical pitch of 30–40 μm and are capable of emitting wavelengths down to the ultraviolet (UV). The electroluminescence spectrum from such a micro-UV emitter is shown in figure 1(*a*) where a narrow band emission is observable with a maximum at ∼370 nm. With high spatial, spectral and temporal resolution, these micro-structured light sources allow high-frame-rate programmable pattern exposure and excitation for various micro-system applications.

For display, lighting and selected instrumentation applications, full-colour (red-, green-, blue-) and white-light emission are required. The most common way of achieving this is through luminescence down conversion, in which a UV/blue AlInGaN LED pumps one or more visible phosphors and generates secondary (longer-wavelength) luminescence. Traditional phosphors are rare-earth doped metal oxide materials made by high-temperature reactions, and these are typically prepared with grain sizes in the tens of micrometre range [9]. Therefore the phosphor-based approach to colour conversion presents a problem for micro-LED arrays, in which the size of the emitting elements may be comparable to, or even smaller than, the typical grain size of a conventional phosphor.

In parallel to the development of nitride materials and devices, tremendous progress has been made in organic optoelectronic materials such as conjugated light-emitting polymers (LEPs). These low-cost organic materials can be easily processed from solution and can be molecularly engineered to emit at different wavelengths [10]. Therefore, conjugated LEPs are a suitable class of materials for AlInGaN LED luminescence down conversion [11]. The benefits of combining organic conjugated materials with nitride LED excitation have been identified recently. It is anticipated that hybrid (organic/nitride) micro-structured LED devices will take full advantage of the optical and electronic properties of both organic and nitride materials and offer a promising route to development of a range of low-cost and highly efficient micro-light sources.

In contrast to organic dyes and small-molecule metal complexes, which can also be used for down conversion [12–14], conjugated polymers are relatively free from concentration quenching effects. This means that high chromophore densities can be used to produce more compact structures. The polyfluorenes have emerged as an attractive alternative to other polymers, owing to their high fluorescence quantum efficiencies and that they are the only currently available family of conjugated polymers to offer a range of available emission wavelengths that spans the entire visible spectrum [15–17]. Their development as commercial electroluminescence materials has also meant that their synthesis and purification has been optimized to yield high chemical purity and reproducibility [15].

Four polymers were chosen for use in hybrid devices: poly(9,9-dioctylfluorene) [PFO], poly(9,9-dioctylfluorene-*co*-9,9-di(4-methoxy)phenylfluorene) [F8DP], two blue emitters; poly(9,9-dioctylfluorene-*co*-benzothiadiazole) [F8BT], a green emitter and the Sumitomo proprietary red emission copolymer Red F. These materials were selected for their high solid-state photoluminescence efficiencies and their ability to cover together the entire visible spectrum [17]. The absorption spectra of F8DP, F8BT and Red F are shown in figure 1(*a*). The F8DP absorption is a broad featureless band that peaks at 390 nm, similar to that of poly(9,9-dioctylfluorene) [PFO] [18], the prototype of this family of polymers. The absorption spectra of F8BT and Red F are similar to each other, with pronounced maxima at about 330 and 455 nm. The Red F spectrum is, however, distinguishable by a weaker absorption feature at 550 nm and a shoulder at 400 nm due to the presence of a red emitting chromophore.

The only criterion for developing hybrid devices based on radiative transfer is that there should be absorption by the polymer of photons emitted by the AlInGaN LED and that the polymer should efficiently convert this energy into photons at

longer wavelengths. It is clear from the LED emission and the absorption of the polyfluorene materials in figure 1(*a*) that F8DP is an excellent candidate for making a hybrid device (due to a large overlap at the absorption maximum). Although the LED emission does not coincide with their absorption maxima, F8BT and Red F also represent good prospects for fabricating hybrids. In the case of these materials, it would be better to use a longer-wavelength LED source (e.g. the 460 nm LED micro-arrays demonstrated in [4]). However, for the purposes of this work and in particular for the white light generation experiments, only 370 nm LED structures were used.

By using polyfluorene materials integrated with the AlInGaN micro-LED array, it is possible to create full-colour rendering hybrid micro-displays that down-convert the emission from the UV to visible wavelengths via radiative energy transfer. These hybrid micro-displays have the potential to be used in a range of associated devices for scientific and instrumentation purposes. Stability of emission will be a determining factor in assessing commercial application and further effort will undoubtedly need to be invested in optimizing packaging (encapsulation) to achieve this goal.

1.2. Hybrids using non-radiative resonant Förster energy transfer

Other hybrids of potential interest are inorganic/organic semiconductor structures designed to utilize Förster resonant energy transfer (FRET) [19] from excitations generated in InGaN/GaN QWs to excitons in the conjugated polymer. In addition to requiring a significant spectral overlap between the InGaN emission and the polymer absorption, these hybrids require that the two materials be placed in close proximity (interaction distance, $R \approx$ few nm). The geometry where an organic energy acceptor material is placed on top of a semiconductor quantum well (QW) energy donor, with a thin spacer, is predicted to exhibit efficient FRET [20, 21]. Structures like this, where the two materials are prepared in a controlled, stratified architecture provide an ideal system to study the interesting, yet experimentally rather unexplored, nature of non-radiative interactions between inorganic Mott–Wannier (M–W) excitons and organic Frenkel excitons. Hybrids using this scheme have the potential to be considerably more efficient in terms of energy transfer than their radiative energy transfer counterparts. A schematic of the structures used for photo-pumped FRET demonstrations in the current work is shown in figure 1(*c*).

Due to the more stringent requirements for demonstrating FRET some attention needs to be paid to the choice of QW as well as the polymer layer. As has already been seen InGaN emission can be tuned to provide excellent spectral overlap with F8DP [22]. Consequently, hybrids were fabricated, by preparing specifically tailored InGaN/GaN single QWs, each with a thin GaN cap (approximate thickness 2.5–15 nm) and then depositing a thin layer of F8DP (approximate thickness 5–10 nm) on top of this structure. By altering the GaN cap thickness it is then possible to change the separation distance between the QW and polymer, and thereby control the FRET process. The FRET process is dependent on the GaN cap thickness resulting in a significant enhancement in the F8DP emission (relative to that for simple radiative transfer) for small separation distances. The associated non-radiative processes in these structures are studied in detail using a combination of low-temperature spectrally and temporally resolved optical measurements, supported by structural characterization. Using this approach it is possible to directly observe changes in the flow of energy out of the QW and to correlate these with changes in emission from the polymer layer. These results exclude the possibility that a significant fraction of the energy from the QW is dissipated in non-radiative centres such as surface states or interface defects and consequently confirm the anticipated non-radiative transfer process. Analysis of the data also reveals that the resonant Förster coupling between the inorganic M–W and the organic Frenkel excitons is best characterized by a plane–plane interaction. The temperature dependence of the structures is also studied, revealing that the FRET process becomes significantly more efficient at high temperatures, making this a favourable mechanism for use in real device structures. In order to access other colours and in particular for white light generation FRET structures are used where energy transfer from an InGaN/GaN QW occurs into a blend incorporating F8DP, F8BT and Red F, with energy transfer within the blend then controlling the relative proportions of red, green and blue light and hence to match to white light.

2. Experimental

2.1. Radiative energy transfer devices

Two techniques have been developed to fabricate the hybrid LED devices. One is to integrate continuous polyfluorene films with micro-pixellated LEDs as shown in figure 1(*b*) and another is to fabricate and integrate polyfluorene blend microstructures with micro-stripe LEDs by UV light 'direct writing'.

2.1.1. Hybrid LEDs with continuous polyfluorene films. For this approach, the inorganic component of the hybrid devices comprises a micro-pixellated UV (370 nm) AlInGaN LED, consisting of a two-dimensional array of 64 × 64 micro-LED elements fabricated in a matrix-addressed format. The fabrication of this micro-array UV LED structure was presented in detail elsewhere [3] as are its emitted beam characteristics in bare chip format [7]. The individual micro-LED elements in the array have a diameter of 20 μm and a centre-to-centre spacing of 30 μm, and can produce an output power of about 1 μW per element. Polymer films of ∼200 nm thickness were formed by spin coating from 20 mg ml^{-1} toluene solutions onto carefully cleaned quartz substrates and then brought into contact with the InGaN-based LED structure (polymer side facing the LED). Following optical excitation by the UV LED emission, the longer-wavelength photoluminescence (PL) generated from the polymer films was detected using a fibre-coupled spectrograph equipped with a charge coupled device (CCD) detector.

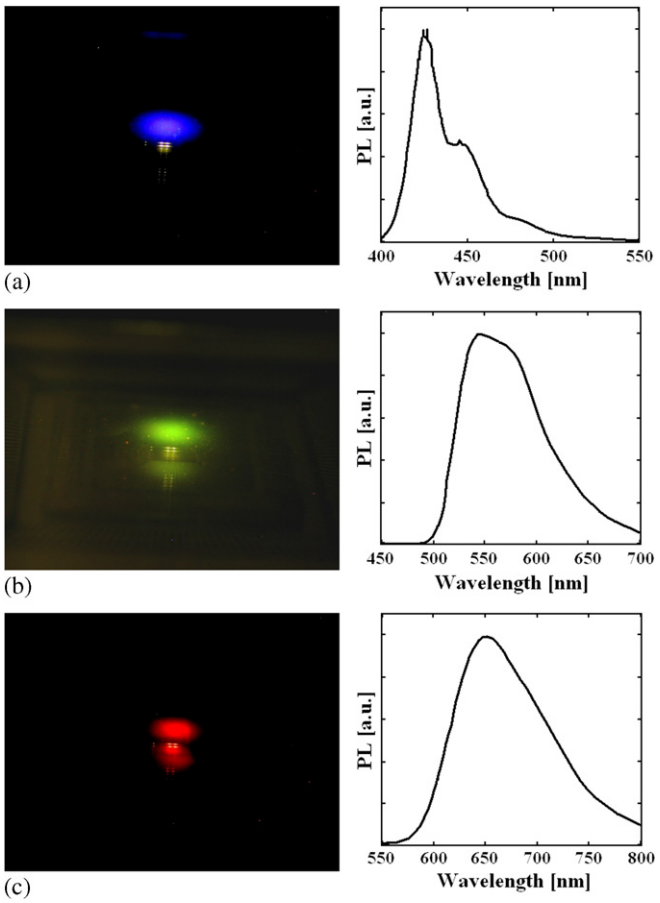

Figure 2. Vertical emission patterns with measured photoluminescence spectra from the (*a*) F8DP, (*b*) F8BT and (*c*) Dow Red F-based hybrid LEDs.

For the production of white light-emitting hybrid LEDs, rather than opting for the more conventional complex multilayer structures (in which the different polymer layers produce emission of different colours that subsequently mix), a blend (F8DP, F8BT and RedF) has been employed. This approach takes advantage of a complimentary overlap between the absorption and emission features of these polymers (see figures 1 and 2) so that the blend can support incomplete non-radiative resonant energy transfer thus allowing all three colours to be emitted. Using this approach takes full advantage of the chemical properties of conjugated polymers and can dramatically reduce fabrication time and complexity (see figure 3(*a*)). An important issue, though, is to ensure that the blend morphology remains stable over time since the energy transfer and hence emission colour is highly sensitive to the microstructure. To fabricate the blends, stock solutions of all three polymers were made up in toluene (20 mg ml^{-1}) from which the appropriate volumes were then extracted and mixed to give the desired blend solutions. The blend composition was carefully adjusted for balanced white light emission. In these systems, F8DP is the host polymer and both F8BT and Dow Red F act as guest emitters to which energy transfers. The concentration of F8DP was varied between 98 and 99 wt%, whereas the F8BT and Dow Red F content ranged between 0.4 and 1.6 wt%.

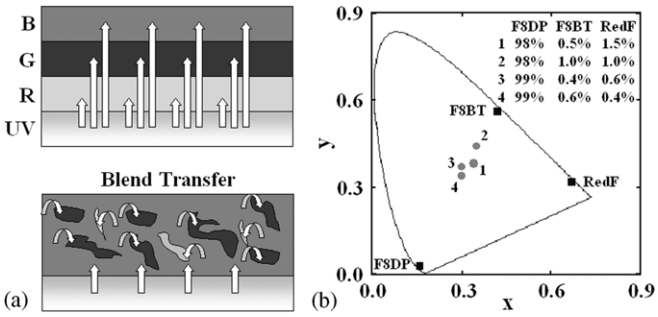

Figure 3. (*a*) Potential structures for white light emission. A multilayered structure allows for radiative pumping of all RGB polymer components. A blend can also be pumped where the blue is excited and an internal energy transfer process redistributes excitons to the green and red emitters. (*b*) CIE (1931) coordinates for the polymer blend hybrid LEDs (devices 1–4, with the blend composition as indicated). Also shown are the CIE coordinates for structures based on pure F8DP, F8BT and Dow Red F (shown).

2.1.2. Hybrid micro-stripe LEDs fabricated by 'direct writing'. The inorganic component of these hybrid devices is a UV (370 nm) LED array, consisting of 120 individually addressable, parallel micro-stripe elements [8, 23]. Although this approach of fabricating hybrid inorganic/organic micro-structured LED devices is demonstrated by using a micro-stripe format array, alternative hybrid devices with different formats such as micro-discs and rings can be achieved in a similar way.

To fabricate the hybrid inorganic/organic LED devices, the blue light-emitting poly(9,9-dioctylfluorene) [PFO] conjugated polymer in a 20 mg ml^{-1} solution of toluene was mixed with a divinyl functionalized monomer and a photoacid generator (0.05 wt% relative to the monomer) in solution. A concentration of PFO equivalent to 0.3 wt% (including solvent) relative to the monomer was found to achieve high curing definition. Other LEPs including blue-emitting poly(9,9-dioctylfluorene-*co*-9,9-di (4-methoxy) phenylfluorene) [F8DP] and the green-emitting poly(9,9-dioctylfluorene-*co*-benzothiadiazole) [F8BT] were also used to make photocurable blends for hybrid device fabrication.

The polyfluorene/divinyl monomer/photoacid mixture blend was spin-coated directly on the surface of the UV micro-stripe LED device. Polymer microstructures were then formed by local photo-curing using the individual micro-UV beams generated from the micro-stripe LED elements underneath the blend layer. For a single LED stripe, an injection current of 5.0 mA was used, which gave an optical output power of 18 μW. An optimized curing time of 0.5 s was used and under these conditions, the energy dose for polymer curing is estimated to be 15.7 mJ cm^{-2}. The unexposed regions of the blend layer were then removed by washing in toluene to leave a single integrated polymer stripe. The polymer microstructure fabricated in this way had a thickness of 20 μm.

2.2. Preparation and study of FRET structures

The QW structures were grown by metalorganic vapour phase epitaxy (MOVPE) on single-side polished (0 0 0 1)-oriented sapphire substrates, in consecutive growth runs in an Aixtron

200/4 RF-S reactor. The nitride hetero-structures grew in the hexagonal wurtzite phase, with the unique *c*-axis in the surface normal direction. They differ only in the thickness of the GaN cap above the QW, which was controlled as described below. More details are published elsewhere of the generic QW growth conditions [24] and photoluminescence (PL) characterization of these particular samples in the as-grown state [25]. However, a few growth parameters significant for the FRET study are summarized here. The growth sequence started by depositing a $\sim$2 μm thickness layer of high-temperature GaN (HT-GaN), at a set-point temperature of 1130 °C. The InGaN/GaN QWs (of nominal thickness 2.5 nm) were grown directly on the surface of the HT-GaN buffer layer, following a growth interruption to allow cooling to a set-point temperature of 860 °C. Finally, the GaN cap layer was grown at the same temperature as the QW growth, without a further interruption. The nominal cap layer thicknesses quoted assume exact proportionality between the growth period and the resulting thickness, and a (kinetically limited) growth rate of 100 nm h^{-1}. Structures for FRET studies were prepared by spin coating F8DP from a 4 mg ml^{-1} toluene solution onto InGaN/GaN QW structures with nominal cap layer thicknesses of 15, 4 and 2.5 nm henceforth designated hybrids A, B and C. For the preparation of white light-emitting FRET structures a polymer blend (98.4% F8DP, 1% F8BT and 0.6% RedF) layer was spin cast from a 4 mg ml^{-1} toluene solution in place of the F8DP.

Atomic force microscopy (AFM) measurements on as-grown QWs were performed with a commercial MultiMode scanning probe microscope (MultiMode Nanoscope IIIA, Digital Instruments). Surface imaging was performed in a non-contact, tapping mode (resonant frequency 190 kHz) at a scanning speed 1–5 μm s^{-1}. Ultra-sharp tips, with a radius of curvature $\sim$2 nm were used (cf standard tip radius of curvature is 5–10 nm). Rutherford backscattering (RBS) measurements, used here for experimental determinations of the GaN cap layer thicknesses, are described in detail in [26].

For PL excitation, hybrids were pumped at close to normal incidence using a Q-switched Nd : YAG laser pumped type-II BBO optical parametric oscillator (10 ns pulses, 10 Hz at 360 nm). For lifetime measurements the hybrids were excited using the frequency-doubled output of a mode-locked Ti : sapphire laser (150 fs, 76 MHz). The PL was spectrally and temporally resolved using a CCD and a streak camera (25 ps resolution), respectively. Measurements presented here were obtained from samples held at a temperature in the 8–75 K range using a liquid helium optical cryostat.

3. Results and discussion

3.1. Selectable colour and white light-emitting devices based on radiative transfer

3.1.1. Emission from the hybrid LEDs with continuous polyfluorene films. Figure 2 shows emission images of the three hybrid LEDs with continuous polyfluorene films as well as the corresponding emission spectra from these devices based on F8DP, F8BT and Dow Red F, respectively. The blue emission from the F8DP-based down-conversion LED has Commission Internationale de L'Eclairage (CIE 1931) (x, y) coordinates (0.16, 0.03). This device exhibits a structured emission spectrum that shows well-defined peaks at 425, 450 and 480 nm (corresponding to the F8DP vibronic structure). The F8BT and Dow Red F-based down-conversion LEDs produce green-yellow and red emission, respectively. The emission from the F8BT based device has CIE (1931) (x, y) coordinates (0.42, 0.56) and exhibits a peak at 545 nm, a shoulder at 576 nm and a long-wavelength tail that extends up to $\sim$750 nm. Finally, the red emission from the Dow Red F-based down-conversion LED has CIE (1931) (x, y) coordinates (0.67, 0.32) and a spectrum that extends from 580 to 850 nm, with a peak at 660 nm. It can be seen that simply changing the organic component of the structures produces hybrid LEDs that exhibit entirely different emission spectra and can operate across the entire visible spectrum. The data presented in this work were obtained by pumping the polymer films with individual elements of the UV micro-LED array. However, it should be noted that the LED array can also provide programmable spatially selective pumping of the polymer film to generate particular emission patterns.

Figure 3(*b*) shows the colour characteristics on a CIE (1931) chromaticity chart of four typical hybrid LEDs that were fabricated using polymer blends. The CIE coordinates of the structures based on pure F8DP, F8BT and Red F are also shown for comparison. The blend emission (devices 1, 3 and 4) appeared white to the eye, while device 2 appeared yellowish-white. Hybrid device 4 was the closest to the zero saturation white (0.33, 0.33), having coordinates (0.30, 0.34). The emission characteristics of these structures are rather sensitive to even small changes in the blend composition. In addition, the shape of the output spectrum is not linearly related to the blend composition. This can be expected since the white light emission in these systems is facilitated by non-radiative Förster energy transfer involving blue to green, green to red and blue to red transfer processes.

Following excitation by the 370 nm UV LED, a complex emission mechanism follows. The majority of the UV LED emission is absorbed by F8DP, which is the dominant component in the blend. A certain fraction of the resulting F8DP excitations (dependent upon the specific blend composition) produces blue PL, while the remainder are Förster transferred to F8BT and Dow Red F (cf overlap between F8DP PL and 455 nm centred F8BT and Dow Red F absorption peaks in figures 1 and 2). The vast majority of the F8BT excitations then produce green emission. A small fraction of the F8BT excitations are again non-radiatively transferred to Dow Red F (cf F8BT PL and 550 nm centred Dow Red F absorption peak overlap). This step is limited by the blend morphology; since the F8BT and Red F concentrations are small (compared with the F8DP), the domains of these materials are likely to be significantly phase separated from each other (and surrounded by F8DP), thereby preventing energy transfer. Finally, the Dow Red F excitation, created by Förster transfer from both F8DP and F8BT, result in red emission and the process is completed. While the LED is capable of exciting the F8BT and Dow Red F chains directly, the resulting green and red emission is expected to be extremely

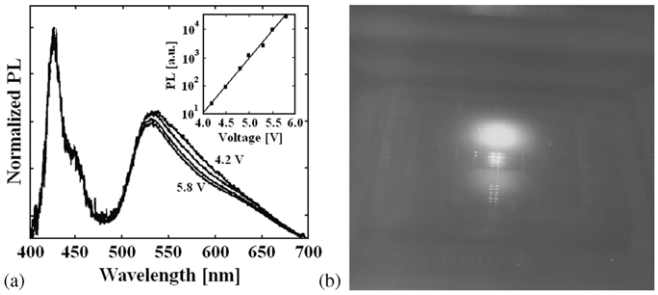

Figure 4. (*a*) White light emission spectra shown as the LED drive voltage is increased from 4.2 to 5.8 V for device 4. The inset shows an exponential fit to the integrated output intensity from this device as a function of driving voltage, indicating diode behaviour. (*b*) Optical micrograph showing the white LED operation.

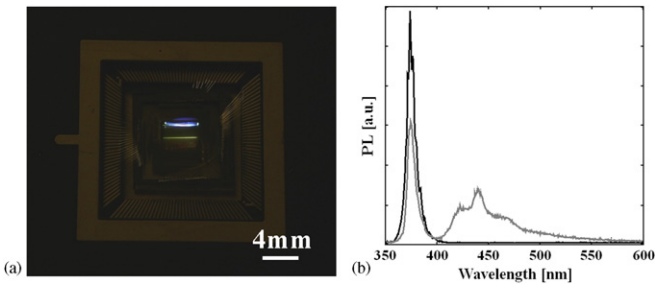

Figure 5. (*a*) Optical micrograph of an operating hybrid micro-stripe LED device, showing a turned-on hybrid stripe LED (above) and a turned-on bare stripe LED (below). (*b*) Emission spectrum of a bare UV LED stripe (black line) and a hybrid stripe LED (grey line).

weak due to the very low F8BT and Dow Red F content in the blend films. This has been verified by selectively pumping both of the guest components of the blend system in turn using a SPEX FluoroMax 3 spectrofluorimeter.

The inset to figure 4(*a*) shows the wavelength-integrated output signal from hybrid device 4 as a function of LED driving voltage. It can be seen that the signal grows exponentially with increasing voltage (typical diode behaviour) and that no saturation occurs. The emission spectrum from the hybrid device does, however, show a small dependence on LED voltage. This is shown in figure 4(*a*), where spectra for the hybrid device are presented at a variety of driving voltages. It can be seen that the blue emission slightly increases relative to the green-red part of the emission for increasing voltages. This may be due to saturation of the energy transfer process. The observed changes in the spectra are, however, very small, especially when compared with the emission from white organic LEDs that are typically much more highly voltage dependent.

3.1.2. Emission from the hybrid stripe LEDs fabricated by 'direct writing'. An operational image of a fully packaged hybrid inorganic/organic micro-stripe LED array fabricated by self-aligned writing is shown in figure 5(*a*). In figure 5(*a*), for comparison purposes, the turned-on lower stripe is a bare UV micro-LED element and the turned-on upper stripe has the photo-cured polymer blend microstructure on top of a LED stripe. This image shows that the UV LED stripe that 'wrote' the stripe pattern into the blend film is fully covered by the polymer stripe, demonstrating the capability of direct writing and self-alignment. The automatically aligned polymer micro-stripes serve as wavelength converters, absorbing photons from the InGaN/AlGaN quantum wells and then re-emitting photons at longer wavelength (with the characteristic spectrum of the chosen conjugated LEP) thus forming a hybrid inorganic/organic micro-stripe LED device.

With PFO LEPs, the hybrid micro-stripe LEDs emit in the blue spectral region. The resulting emission spectrum for this hybrid micro-structured LED device was measured and is shown in figure 5(*b*) together with the electroluminescence spectrum of a bare LED micro-stripe. It has been shown that the vinyl polymer alone has negligible photoluminescence [23]. From figure 5(*b*), it is evident that the emission characteristics of the hybrid micro-stripe LED in the visible region closely match those of the pure PFO layer. The blending and photo-curing processes do not, therefore, substantially alter the emission characteristics of the PFO within the organic micro-stripe of the hybrid device. Due to the low concentration of PFO in the organic micro-stripe, combined with the high UV transparency of the vinyl ether polymer, the transmitted 370 nm emission is clearly seen in the emission spectrum of the hybrid LED device. This UV emission would allow further writing for example to create a multilayer microstructure for white light emission. Otherwise it would be possible to filter it with a variety of conventional polymer coatings.

3.2. Structural characterization of FRET structures

For rigour in the mechanistic analysis of the FRET process presented in section 3.5, it is essential to understand the surface morphology of the as-grown InGaN/GaN QWs, and to have experimental checks of the thickness of the GaN cap layer. The nucleation and subsequent growth of the HT-GaN buffer layers on the sapphire substrates was carefully controlled to give a morphology characterized by atomically flat terraces, and so-called 'monolayer' steps [27]. These have a height of half the GaN *c* lattice constant, corresponding to a value of ∼0.26 nm. This buffer layer morphology is standard for optimized GaN growth by MOVPE on (0 0 0 1)-oriented sapphire [28, 29]. It has been established that the morphology of InGaN/GaN QW structures grown at lower temperatures may not necessarily replicate that of the GaN buffer layer, depending on the exact growth conditions, and new morphological features can develop [29–31]. However, the growth regime employed in this study did in fact preserve a surface consisting of atomically flat terraces ∼100 nm in width, as evidenced by the AFM image shown in figure 6. Root mean square (RMS) roughness values and other parameters extracted from the AFM analyses on the three samples with the different cap layer thicknesses are summarized in table 1. Experimental measurements of the mean GaN cap layer thicknesses were made by a RBS method described in detail elsewhere [26]. In brief, this involved exploiting the enhanced depth resolution obtained by using grazing incidence for the incoming ion beam, and measuring the shift in the indium scattering peak caused by

the energy loss of ions traversing the GaN cap layer. The RBS-derived thickness values are averages over a macroscopic area, since the beam spot size on the sample was ∼1 mm diameter. The resulting values, and uncertainties, are summarized in the right-hand column of table 1. The RBS measurements also allowed the QW thicknesses and compositions to be checked; a mean thickness of 2.2 nm, and an alloy composition of $In_{0.07}Ga_{0.93}N$, provided a self-consistent analysis.

3.3. Optical characterization of FRET structures

Figure 7 shows the time-integrated PL emission spectra obtained from the hybrid structures at a temperature of 15 K. The spectra contain peaks from the QWs at 387 nm, 397 nm and 388 nm for hybrids A, B and C, respectively, and from the polymer at 425 nm and 455 nm (vibronic peaks). The variation in the QW emission wavelengths is within the range expected due to differences in well composition and thickness. Furthermore, they are not significant to our studies because the broad absorption peak of the polymer ensures that the spectral overlap of the QW emission and polymer absorption is comparable in all cases. Measurements made before depositing the F8DP layer revealed similar integrated PL intensities for all three QWs despite the differences in GaN cap thickness. However, in the hybrid heterostuctures, the relative QW PL intensity is reduced with decreasing cap thickness while the relative polymer PL emission is simultaneously increased. Similar cap-dependent variations in the relative intensities of the QW and polymer emission were seen in spectra obtained from the hybrid structures across the whole 8–75 K temperature range studied. The observed quenching of the QW PL emission and accompanying enhancement of the polymer PL provide clear evidence for non-radiative energy transfer from the QW to the polymer. Any radiative energy transfer would be independent of cap thickness and should not lead to a modification of the QW emission intensity. A potential source of the observed PL behaviour is that charge (in particular electrons) could transfer from the InGaN/GaN QW to the polymer layer. However, such a process is strongly inhibited by the large energy offset at the GaN/F8DP interface that results in a barrier of the order of 1.5 eV [32,33]. Enhancement of the polymer PL emission due to any (unknown) effects at the GaN/F8DP interface have been previously eliminated by appropriate control experiments with an InGaN/GaN QW emitting at ∼500 nm [34].

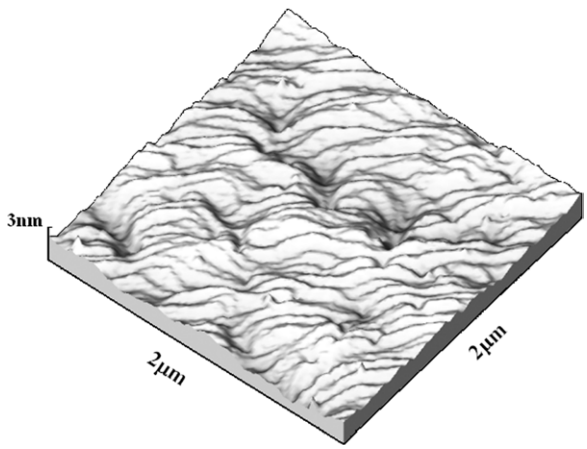

Figure 6. Three-dimensional height-scaled AFM image of the as-grown InGaN/GaN QW sample C, with the thinnest GaN cap layer.

3.4. Study of the dynamics of FRET

The time dependence of the QW PL data at 15 K contains both short- and long-lived decay components (see figure 8). The short-lived decay is attributed to the spectral overlap of the laser pulse tail with the QW emission and defines the resolution of the measurement. The long-lived component represents the recombination decay of the QW. The dynamics of the system can therefore be modelled over the course of time, t, as $e^{-k_l t} + e^{-k_{qw} t}$, where k_l is representative of the laser excitation and k_{qw} is the QW recombination decay rate. All decay fits to the data using this model obtain the same value for $k_l = 40\ ns^{-1}$ with standard deviation from the fitting procedure of less than 1.5%. As would be expected, this value of k_l corresponds to a laser pulse duration of 25 ps, the aforementioned resolution of the streak camera.

The recombination rate of a QW, in the absence of a polymer over-layer, can be written as

$$k_{qw} = k_r + k_{nr} \tag{1}$$

while in the case of a hybrid QW the recombination rate is written as

$$k^h_{qw} = k_r + k_{nr} + k_F, \tag{2}$$

where the radiative and non-radiative decay rates are k_r and k_{nr}, respectively, while k_F is the characteristic Förster transfer rate from the InGaN/GaN QW to the polymer layer. The values for k_{qw} and k^h_{qw}, obtained from the fitting procedure are summarized in table 2. The recombination decay rates of the QWs in the absence of polymer over-layers correspond to decay lifetimes (NB $k = \frac{1}{\tau}$) of between 0.72 and 0.92 ns. Recombination lifetimes in the 0.5–0.8 ns range have been reported previously for similar single InGaN/GaN wells [35,36] at low temperature, in good agreement with the results obtained here, and are thought to be due to exciton

Table 1. Parameters extracted from AFM analysis of as-grown InGaN/GaN QWs, plus the most probable cap thickness values, with uncertainties, derived from RBS measurements.

Hybrid	RMS roughness (nm)	Mean terrace width (nm)	Mean step height (nm)	Cap thickness from RBS(nm)
A	1.1	94	0.4	11.8 ± 0.8
B	0.6	100	0.3	3.2 ± 0.5
C	0.3	92	0.5	1.9 ± 0.5

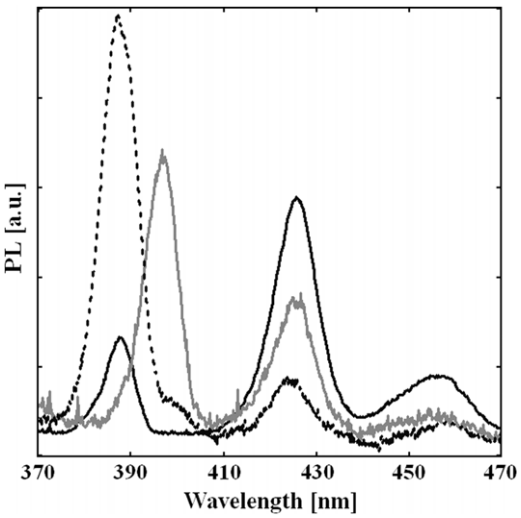

Figure 7. Time-integrated photoluminescence (PL) spectra. Data are shown for hybrids A (black dashed line), B (grey line) and C (black line) at 15 K. As the cap thickness is decreased the polymer emission is increased at the expense of the QW emission, indicating energy transfer.

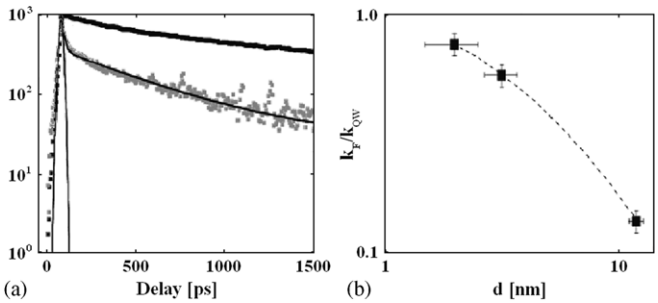

Figure 8. 15 K QW PL decay curves without (black points) and with (grey points) the F8DP over-layer for (*a*) hybrid C on a semi-logarithmic plot. The bi-exponential fitting curves of the decays and the excitation laser pulse are also displayed (black solid lines). The dependence of the normalized Förster rate (k_F/k_{QW}) on the cap thickness d is shown on a log–log scale in (*b*) together with a quadratic fit (using equation (4) with $P = 2$).

Table 2. Radiative QW decay rates in the absence of polymer over-layers (k_{qw}), radiative QW decay rates in the presence of polymer over-layers (k^h_{qw}) and estimated Förster transfer rates (k_F) for the InGaN/F8DP hybrid samples.

Hybrid	k_{qw} (ns^{-1})	k^h_{qw} (ns^{-1})	k_F (ns^{-1})
A	1.10	1.27	0.17
B	1.39	2.17	0.78
C	1.30	2.27	0.97

recombination processes in the wells. The modest variation in lifetime is within the range expected for sample-to-sample variations in well composition and thickness.

It is evident from table 2 that the QW recombination rate for the hybrid samples, k^h_{qw}, is noticeably greater than for the QWs measured in the absence of an overlying polymer layer. The reduction in the PL of the QW for hybrids of decreasing cap thickness indicates that there is an additional non-radiative decay channel, which is dependent on the separation distance from the polymer. This behaviour is strongly indicative of a resonant energy transfer process. Using equations (1) and (2), it is possible to evaluate the FRET transfer rate from the hybrid decay rate and that of the original QW

$$k_F = k^h_{qw} - k_{qw}. \tag{3}$$

It is clear from table 2, that this evaluated FRET rate increases significantly as the cap thickness is reduced. Using the deduced values of k_F and k_{qw} at 15 K leads to estimated FRET efficiencies $\Phi_F = k_F/(k_F + k_{qw})$ of $13.4 \pm 1.1\%$, $36.4 \pm 2.9\%$ and $42.8 \pm 3.4\%$ for hybrids A, B and C, respectively, i.e. increasing efficiency with decreasing cap thickness.

3.5. Mechanistic nature of the FRET transfer process

Further understanding of the nature of FRET coupling between the InGaN/GaN QW and F8DP can be gained by adopting a procedure used in a previous study of FRET between two different polyfluorene layers separated by a variable-thickness inert spacer [37]. The ratio of the FRET and quantum well decay rates (k_F and k_{QW}, respectively) can be written as a function of the interaction distance R:

$$k_F/k_{qw} = (R_F/R)^P, \tag{4}$$

where R_F is the Förster radius (at which spacing the rates are equal). The spacing between the donor and acceptor $R = d+x$, where d is the GaN cap layer thickness (as measured by RBS) and x is an adjustable correction factor (associated with the finite width of the QW and F8DP layers) that, when added to the measured cap thickness, accounts for the average dipole–dipole separation. The appropriate exponent P depends on the nature of the dipole–dipole interaction with $P = 2$ representing layer-to-layer coupling (2D to 2D), $P = 4$ the coupling between a point dipole and a layer (0D to 2D) and $P = 6$ the coupling between two point dipoles (0D to 0D). The dependence of k_F/k_{qw} at 15 K on the GaN cap layer thickness d, as well as the fitted curve for $P = 2$ are shown in figure 8(*b*). The horizontal and vertical error bars represent, respectively, uncertainties in the RBS-derived cap thickness values (see table 1) and the variation in the QW decay lifetimes at different locations on each sample (measurements in the absence/presence of the F8DP over-layer were not made at identical locations). The deduced fitting parameters, R_F and x, for the three different dipole–dipole geometries are listed in table 3. Given the measured (by the RBS measurements) QW thickness of 2.2 nm and the F8DP nominal layer thickness of 5 nm the x-values for $P = 4$ and $P = 6$ are unreasonably large whilst that for $P = 2$, namely, $x = 4.8 \pm 0.9$ nm, is quite plausible. Similarly, the Förster radius for $P = 2$, namely, $R_F = 6.1 \pm 0.8$ nm, is in reasonable keeping with typical Förster radii for polymer-to-polymer and polymer-to-molecule energy transfer ($R_F \sim$ 3–5 nm [37, 38]). The R_F values obtained for the $P = 4$ and $P = 6$ fits are, however, significantly larger. It is clear then that the energy transfer in these structures is best described by a $P = 2$ dependence, indicative of layer-to-layer dipole coupling. The relatively weak dependence on R also suggests that short-range multi-pole interactions such as dipole-quadrupole or exchange

Table 3. Fitting results of the dependence of the normalized FRET rate on the cap thickness values for different values of P.

Model Parameters (nm)	$P = 2$ (2D to 2D)	$P = 4$ (0D to 2D)	$P = 6$ (0D to 0D)
R_F	6.1 ± 0.8	16.5 ± 0.2	27.1 ± 3.3
X	4.8 ± 0.9	15.2 ± 3.1	25.6 ± 5.8

coupling do not significantly contribute to the energy transfer in these hybrids. Further experimental studies addressing a wider parameter space should prove helpful in better characterizing the energy transfer process, as indeed should complementary theoretical studies.

3.6. Temperature dependence of FRET efficiency

It has been implicitly assumed that the non-radiative transfer described above involved M–W excitons. This is plausible as the binding energy of M–W excitons in InGaN/GaN QWs is larger than kT even at room temperature ([39], for example, quotes a calculated exciton binding energy of 53 meV for InGaN/GaN QWs with similar parameters to those studied here). On the other hand, the combination of spontaneous (pyroelectric) polarization in the wurtzite-phase nitrides, and piezoelectric effects in the compressively strained QW material, implies that strong electric fields running along the [0 0 0 1] direction through InGaN/GaN QWs could cause separation of the electron and hole wave-functions [40]. The dominant radiative mechanism becomes band-to-band recombination in these circumstances. Excitons may be localized by impurities or well width variations at low temperature but become delocalized at intermediate temperatures. Consequently, a study of FRET across a wider temperature range may be useful. From the time resolved results it can be seen that hybrid A had a relatively small energy transfer rate and thus can be considered a suitable control sample for gauging the enhancement due to FRET versus the radiative energy transfer process. Figure 9 shows the integrated emission intensity ratios I_C/I_A and I_B/I_A throughout the temperature range 77–300 K, where I_A, I_B and I_C are the F8DP integrated PL intensities measured for hybrids A, B and C, respectively. Before integration the recorded spectra were corrected for the background polymer emission that arises from direct pump laser excitation, by subtracting the polymer emission observed for a 5 nm F8DP film deposited on a fused silica substrate. Consequently, the ratios represent the intensity enhancement due to FRET compared with radiative transfer from the QW to the F8DP film. At temperatures up to ~175 K the intensity enhancement is roughly constant with values of 6 and 1.75 for I_C/I_A and I_B/I_A, respectively. At higher temperatures, these ratios increase monotonically to 20 and 4 at 300 K.

The general evolution with temperature of the dominant type of excitation in InGaN/GaN QWs is now generally agreed [39, 41, 42], and is pertinent to the interpretation of the results in figure 9. At low temperatures, excitons localized at potential minima are dominant. As the temperature increases, these excitons escape from the potential minima, and become

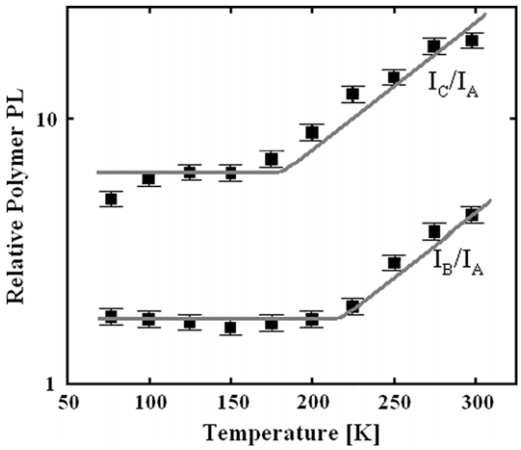

Figure 9. Integrated intensity ratios I_C/I_A and I_B/I_A versus temperature, where I_A, I_B and I_C are the F8DP PL intensities from hybrids A, B and C, respectively. Note the different behaviour of the energy transfer at low and high temperatures with an onset of temperature dependence at ~175 K.

so-called 'free excitons', although the temperature at which this process occurs depends on the specific QW parameters, i.e. thickness and alloy composition [41]. At sufficiently high temperatures, and/or high excitation rates, free carriers become dominant. Power-dependent PL measurements on the as-grown InGaN/GaN QWs used in this study from 77 to 225 K and at excitation densities of ~1 to 100 μJ cm^{-2} suggest that radiative recombination remains excitonic in character over this full range of conditions. Therefore, the asymptotic behaviour of the energy transfer process in the 77–175 K temperature range can be attributed to the presence of localized excitons in the InGaN/GaN QW, suggesting that delocalized excitons result in a more efficient energy transfer process. The increase in energy transfer efficiency at temperatures greater than ~175 K may be explained by the work of Kos *et al* [39] where the radiative recombination rate was calculated to reduce faster with temperature than the Förster transfer rate. Herz *et al* [43] also noted that the FRET rate was significantly higher at room temperature than at 7 K for a conjugated polymer guest–host system. Consequently, it can be seen that the transfer rate becomes increasingly important as the temperature is raised.

It is instructive to compare the transfer efficiency of FRET with the radiative transfer mechanism at low and high temperatures (15 and 300 K are arbitrarily chosen for this discussion). The radiative transfer emission efficiency, Φ_r, is given by

$$\Phi_r \approx \eta_p \Phi_{qw}, \tag{5}$$

where η_p is the fraction of photons emitted by the QW that are absorbed and re-emitted by the F8DP polymer over-layer and Φ_{qw} is the internal quantum efficiency for emission from the QW. The latter depends on the absorption coefficient of F8DP at the QW emission wavelength and the polymer film thickness. Using a value of 3×10^5 cm^{-1} for the F8DP absorption coefficient at 390 nm [44] and taking into account Fresnel reflection at the GaN/F8DP interface (~4.5 % from the refractive indices $n_{F8DP} = 1.7$ and $n_{GaN} = 2.6$ at 390 nm), η_p can be estimated to be ~6.5%. This was obtained using the

Table 4. Transfer efficiencies for a 2.5 nm cap hybrid at 15 and 300 K. The radiative energy transfer efficiency (Φ_r) has been calculated from equation (5). The FRET efficiency (Φ_F) at 15 K was determined from QW decay rate (see section 3.4) while the 300 K value has been estimated (see text). Also shown are the enhancements (I_C/I_A) from figure 9 at both temperatures.

Temperature (K)	Φ_r (%)	Φ_F (%)	Enhancement
15	6.5	43	6
300	0.6	∼12	20

simplification that the well emission is isotropic and thus at least half of the light emitted by the QW does not go through the polymer layer. On the other hand, the InGaN/GaN QW internal quantum efficiency is strongly temperature dependent, ranging from values approaching 100% at 15 K to values that are ∼10% at 300 K. Using these values for η_p and Φ_{qw}, and assuming η_p to be essentially temperature independent, the radiative transfer efficiency (Φ_r) for the hybrids can be evaluated and is listed in table 4. The FRET efficiencies are also shown in table 4, where the 15 K value was obtained from the QW decay dynamics described herein. Due to a low hybrid PL signal it was not possible to directly measure Φ_F at 300 K, however the FRET efficiency can be inferred from the enhancement data in figure 9. At 300 K the FRET process is at least 20 times more efficient than radiative emission so that $\Phi_F \approx 20\Phi_r$. This assumption is supported by the efficiencies at 15 K where Φ_F is seen to be 6.6 times greater than Φ_r, in good agreement with the low temperature enhancement data in figure 9. While the enhancement due to FRET is significantly higher at 300 K, it is worth noting that the overall PL signal is significantly decreased compared with the hybrid at 15 K. It should be noted that Φ_{qw} at room temperature is governed by the nature of the quantum well excitations (bound, free excitons, unbound electron-hole pairs or combinations of all these species) and the complex, temperature-dependent competition of their radiative and non-radiative recombination mechanisms. Consequently, the 10% value used in the analysis above is only a rough estimation of the magnitude of Φ_{qw}, which strongly influences the evaluation of the FRET efficiency Φ_F.

The motivation for using FRET in these hybrids is that it is possible to harvest QW excitations that would normally decay non-radiatively, if radiative transfer was the only down-conversion mechanism present in the hybrids. In the QW, both excitons and free carriers become increasingly susceptible to non-radiative recombination as the temperature increases, which results in the reduction in overall PL emission intensity at 300 K. Since the FRET rate (k_F) is significantly faster than the QW radiative decay rate (k_r), the transfer process can better compete with any non-radiative decay channels, which emerge at higher temperatures. The argument prsented here that the FRET efficiency also increases with the appearance of delocalized excitons at higher temperatures, while further enhancing the energy transfer process over non-radiative decay of QW excitations also highlights the difficulty in modelling the complex processes present in these hybrid structures.

The excited state relaxation within the polymer acceptor occurs on a time scale (hundreds of femtoseconds [45, 46]), which is significantly faster than the FRET time. This means

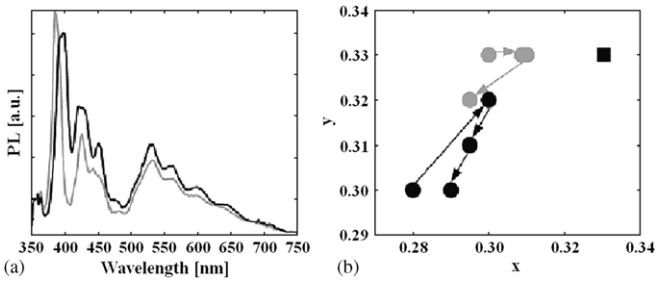

Figure 10. (*a*) PL spectra obtained from hybrid structures, A_{WL} (grey lines) and B_{WL} (black lines) at an excitation density of 580 μJ cm^{-2} (*b*) Variation of the spectral characteristics of hybrid A_{WL} (grey circles) and sample B_{WL} (black circles) with excitation density, displayed on an expanded CIE chromaticity chart (arrows indicate the sequential changes with higher excitation density). The (0.33, 0.33) white light emission point is depicted by the black square.

that the energy transfer is incoherent and no resonant back-transfer of energy occurs to the QW donor. This is known as the weak coupling regime. In the case of strong coupling, coherent exchange of energy between donor and acceptor is expected to lead to the formation of hybrid exciton states [47, 48]. These hybrids would be of great interest to researchers in the field of nonlinear optics and are the subject of ongoing studies.

3.7. White light emission from FRET structures

For simplicity only the data from two white-light emitting hybrid structures are shown (15 and 2.5 nm nominal cap thicknesses) referred to as A_{WL} and C_{WL}, respectively. Figure 10 shows the emission spectra obtained from A_{WL} (grey lines) and C_{WL} (black lines), at an excitation density of 580 μJ cm^{-2}. These spectra represent averages of multiple PL scans at different locations on the hybrid samples to take into account small fluctuations in the well and polymer emission characteristics due to variation of the well width, composition and polymer blend thickness. The emission can be roughly separated into two contributions; PL from the inorganic structure for wavelengths <410 nm and white light emitted by the polymer blend from 410 to 750 nm. The interference fringes visible are caused by Fabry–Perot interference, and have a significant amplitude because of the large refractive index change at the interface between the GaN buffer layer and sapphire substrate. This interpretation is further supported by the fact that the emission from an identical blend film deposited on a glass substrate did not contain any fringes. The excitation processes that occur within the hybrid structure are complex and include direct excitation of the QWs and all three of the blend components by the laser line (see absorption spectra at figure 1(*a*)), radiative pumping of the blend components by the QW, and non-radiative Förster energy transfer from F8DP to F8BT and Red F, as well as from the QWs to F8DP. The first three processes are common to both hybrid structures but the latter process should be stronger for hybrid C_{WL} due to the smaller cap thickness. This is evident from figure 10(*a*), which shows that the well emission is quenched for hybrid C_{WL} relative to hybrid A_{WL}. There is also a simultaneous enhancement of the polymer emission of C_{WL} across the entire

visible range. This indicates that non-radiative transfer of energy occurs from the inorganic well to the polymer blend components and this effect is much stronger when these are in closer proximity.

Finally, the characteristics of white light spectral emission were studied as a function of excitation density from 360 to 920 μJ cm^{-2}. Figure 10(*b*) shows the variation (arrows point towards higher excitation densities) of the emission from hybrid A_{WL} (grey triangles) and hybrid C_{WL} (black triangles) on an expanded CIE chromaticity chart. It is evident that for all excitation values the hybrid emission from the two samples lies close to the (0.33, 0.33) white point identified by the black square. The small variation in the CIE coordinates of hybrid A_{WL} closely resembles the variation observed in the emission from an identical blend film used in the wavelength down-conversion studies, described above. This can be attributed to competition between the non-radiative energy transfer processes, also described above. The observed changes in the spectra of both hybrids are, however, relatively small when compared with the emission from typical structures based on standard phosphor-conversion schemes that are generally more power dependent.

4. Conclusions

Red-, green-, blue and white-light emission from hybrid polyfluorene/InGaN LEDs based on radiative transfer has been demonstrated. Also, it has been shown that it is possible to engineer devices, which make use of efficient Förster resonant coupling between M–W and Frenkel excitons. This work highlights the potential for devices that can access both radiative and non-radiative energy transfer mechanisms to take advantage of the favourable properties of GaN devices and conjugated polymers. Electrically driven QW structures are possible to realize, although there remains the challenge of developing thin-capped QWs, which can simultaneously allow charge injection, while maintaining FRET. This is the subject of ongoing research. It is envisaged that structures based on this approach could have applications for solid-state lighting, biological sensing and potentially hybrid lasers, where electrically driven InGaN-based structures might provide FRET-pumping of organic gain media.

Acknowledgments

We thank the Sumitomo Chemical Co., Ltd for providing the polymers used in this study and Dr J Wilson for useful discussions. We acknowledge Research Councils UK (Basic Technology Research Programme GR/S85764) and the Commission of the European Community (HYTEC IHP Network Project) for financial support.

References

[1] Neher D 2001 Polyfluorene homopolymers: conjugated liquid-crystalline polymers for bright blue emission and polarized electroluminescence *Macromol. Rapid Commun.* **22** 1366–85

[2] Jiang H X, Jin S X, Li J, Shakya J and Lin J Y 2001 III-nitride blue microdisplays *Appl. Phys. Lett.* **78** 1303–5

[3] Jeon C W, Choi H W, Gu E and Dawson M D 2004 High-density matrix-addressable AlInGaN-Based 368 nm microarray light-emitting diodes *IEEE Photon. Technol. Lett.* **16** 2421–3

[4] Jeon C W, Choi H W and Dawson M D 2003 Fabrication of matrix-addressable InGaN-based microdisplays of high array density *IEEE Photon. Technol. Lett.* **15** 1516–8

[5] Ozden I, Diagne M, Nurmikko A V, Han J and Takeuchi T 2001 A matrix addressable 1024 element blue light emitting InGaN QW diode array *Phys. Status Solidi* a **188** 139–42

[6] Jeon C W, Kim K S and Dawson M D 2002 Fabrication of two-dimensional InGaN-Based micro-LED arrays *Phys. Status Solidi* a **192** 325–8

[7] Griffin C, Gu E, Choi H W, Jeon C W, Girkin J M, Dawson M D and McConnell G 2005 Beam divergence measurements of InGaN/GaN micro-array light-emitting diodes using confocal microscopy *Appl. Phys. Lett.* **86** 041111

[8] Zhang H X, Gu E, Jeon C W, Gong Z, Dawson M D, Neil M A A and French P M W 2006 Microstripe-array InGaN light-emitting diodes with individually addressable elements *IEEE Photon. Technol. Lett.* **18** 1681–3

[9] Schubert E F 2006 *Light Emitting Diodes* 2nd edn (Cambridge: Cambridge University Press) pp 351–9

[10] Burn P L, Holmes A B, Kraft A, Bradley D D C, Brown A R, Friend R H and Gymer R W 1992 Chemical tuning of electroluminescent copolymers to improve emission efficiencies and allow patterning *Nature* **356** 47–9

[11] Hide F, Kozodoy P, DenBaars S P and Heeger A J 1997 White light from InGaN/conjugated polymer hybrid light-emitting diodes *Appl. Phys. Lett.* **70** 2664–6

[12] Ermakov O N, Kaplunov M G, Efimov O N, Yakushchenko I K, Belov M Y and Budyka M F 2003 Hybrid organic–inorganic light-emitting diodes *Microelectron. Eng.* **69** 208–12

[13] Guha S, Haight R A, Bojarczuk N A and Kisker D W 1997 Hybrid organic-inorganic semiconductor-based light-emitting diodes *J. Appl. Phys.* **82** 4126–8

[14] Xiang H F, Yu S C, Che C M and Lai P T 2003 Efficient white and red light emission from GaN/tris-(8-hydroxyquinolato) aluminum/platinum(II) meso-tetrakis(pentafluorophenyl) porphyrin hybrid light-emitting diodes *Appl. Phys. Lett.* **83** 1518–20

[15] Bernius M T, Inbasekaran M, O'Brien J and Wu W S 2000 Progress with light-emitting polymers *Adv. Mater.* **12** 1737–50

[16] Inbasekaran M, Woo E, Wu W S, Bernius M and Wujkowski L 2000 Fluorene homopolymers and copolymers *Synth. Met.* **111** 397–401

[17] Xia R, Heliotis G, Hou Y and Bradley D D C 2003 Fluorene-based conjugated polymer optical gain media *Org. Electron.* **4** 165–77

[18] Heliotis G, Bradley D D C, Turnbull G A and Samuel I D W 2002 Light amplification and gain in polyfluorene waveguides *Appl. Phys. Lett.* **81** 415–7

[19] Förster T 1949 Experimentelle Und Theoretische Untersuchung Des Zwischenmolekularen Ubergangs Von Elektronenregungeneragie *Z. Natur. A: Phys. Sci.* **4** 321

[20] Agranovich V M, Basko D M, La Rocca G C and Bassani F 1998 Excitons and optical nonlinearities in hybrid organic-inorganic nanostructures *J. Phys.: Condens. Matter* **10** 9369–400

[21] Agranovich V M, La Rocca G C and Bassani F 1997 Efficient electronic energy transfer from a semiconductor quantum well to an organic material *JETP Lett.* **66** 748–51

[22] Heliotis G, Stavrinou P N, Bradley D D C, Gu E, Griffin C, Jeon C W and Dawson M D 2005 Spectral conversion of

InGaN ultraviolet microarray light-emitting diodes using fluorene-based red-, green-, blue-, and white-light-emitting polymer overlayer films *Appl. Phys. Lett.* **87** 103505

[23] Gu E, Zhang H X, Sun H D, Dawson M D, Mackintosh A R, Kuehne A J C, Pethrick R A, Belton C and Bradley D D C 2007 Hybrid inorganic/organic micro-structured light-emitting diodes produced using photocurable polymer blends *Appl. Phys. Lett.* **90** 031116

[24] Deatcher C J, Liu C, Pereira S, Lada M, Cullis A G, Sun Y J, Brandt O and Watson I M 2003 In situ optical reflectometry applied to growth of indium gallium nitride epilayers and multi-quantum well structures *Semicond. Sci. Technol.* **18** 212–8

[25] Tan L T, Martin R W, O'Donnell K P and Watson I M 2006 Photoluminescence and phonon satellites of single InGaN/GaN quantum wells with varying GaN cap thickness *Appl. Phys. Lett.* **89** 101910

[26] Barradas N P, Alves E, Pereira S and Watson I M 2008 RBS analysis of InGaN/GaN quantum wells for hybrid structures with efficient Förster coupling *Nucl. Instrum. Methods Phys. Res.* B at press

[27] Liu C and Watson I M 2007 Quantitative simulation of in situ reflectance data from metal organic vapour phase epitaxy of GaN on sapphire *Semicond. Sci. Technol.* **22** 629–35

[28] Heying B, Tarsa E J, Elsass C R, Fini P, DenBaars S P and Speck J S 1999 Dislocation mediated surface morphology of GaN *J. Appl. Phys.* **85** 6470–6

[29] Sonderegger S, Feltin E, Merano M, Crottini A, Carlin J F, Sachot R, Deveaud B, Grandjean N and Ganière J D 2006 High spatial resolution picosecond cathodoluminescence of InGaN quantum wells *Appl. Phys. Lett.* **89** 232109

[30] Ting S M *et al* 2003 Morphological evolution of InGaN/GaN quantum well heterostructures grown by metalorganic chemical vapor deposition *J. Appl. Phys.* **94** 1461–7

[31] Suikhonen S, Lang T, Svensk O, Sormunen J, Törmä P T, Sopanen M, Lipsanen H, Odnoblyudov M A and Bougrov V E 2007 Control of the morphology of InGaN/GaN quantum wells grown by metalorganic chemical vapor deposition *J. Cryst. Growth* **300** 324–9

[32] Bougrov V, Levinshtein M E, Rumyantsev S L and Zubrilov A 2001 *Properties of Advanced Semiconductor Materials GaN, AlN, InN, BN, SiC, SiGe* (New York: Wiley)

[33] Janietz S, Bradley D D C, Grell M, Giebeler C, Inbasekaran M and Woo E P 1998 Electrochemical determination of the ionization potential and electron affinity of poly(9,9-dioctylfluorene) *Appl. Phys. Lett.* **73** 2453–5

[34] Heliotis G, Itskos G, Murray R, Dawson M D, Watson I M and Bradley D D C 2006 Hybrid inorganic/organic semiconductor heterostructures with efficient non-radiative energy transfer *Adv. Mater.* **18** 334–8

[35] Chi-Kuang S, Keller S, Tien-Lung C, Wang G, Minsky M S, Bowers J E and DenBaars S P 1997 Well-width dependent studies of InGaN–GaN single-quantum wells using time-resolved photoluminescence techniques *IEEE J. Sel. Top. Quant. Electron.* **3** 731–8

[36] Olaizola S M, Fan W H, Mowbray D J, Skolnick M S, Parbrook P J and Fox A M 2007 Phonon satellites and time-resolved studies of carrier recombination in InGaN qunatum wells *Superlatt. Microstruct.* **41** 419–24

[37] Hill J, Heriot S Y, Worsfold O, Richardson T H, Fox A M and Bradley D D C 2004 Controlled Forster energy transfer in emissive polymer Langmuir–Blodgett structures *Phys. Rev.* B **69** 041303

[38] Virgili T, Lidzey D G and Bradley D D C 2000 Efficient energy transfer from blue to red in tetraphenylporphyrin-doped poly(9,9-dioctylfluorene) light-emitting diodes *Adv. Mater.* **12** 58–62

[39] Kos S, Achermann M, Klimov V I and Smith D L 2005 Different regimes of Forster-type energy transfer between an epitaxial quantum well and a proximal monolayer of semiconductor nanocrystals *Phys. Rev.* B **71** 205309

[40] Waltereit P, Brandt O, Ringling J and Ploog K H 2000 Electrostatic fields and compositional fluctuations in (In,Ga)N/GaN multiple qunatum wells grown by plasma-assisted molecular-beam epitaxy *Phys. Rev.* B **64** 245305

[41] Pecharromán-Gallego R, Martin R W and Watson I M 2004 Investigation of the unusual temperature dependence of InGaN/GaN quantum well photoluminescence over a range of emission energies *J. Phys. D: Appl. Phys.* **37** 2954–61

[42] Hangleiter A, Netzel C, Fuhrmann D, Hitzel F, Hoffmann L, Bremers H, Rossow U, Ade G and Hinze P 2007 Anti-localization suppresses non-radiative recombination in GaInN/GaN quantum wells *Phil. Mag.* **87** 2041–65

[43] Herz L M, Silva C, Grimsdale A C, Mullen K and Phillips R T 2004 Time-dependent energy transfer rates in a conjugated polymer guest–host system *Phys. Rev.* B **70** 165207

[44] Xia R, Heliotis G, Campoy-Quiles M, Stavrinou P N, Bradley D D C, Vak D and Kim D Y 2005 Characterization of a high-thermal-stability spiroanthracenefluorene-based blue-light-emitting polymer optical gain medium *J. Appl. Phys.* **98** 083101

[45] Ariu M, Sims M, Rahn M D, Hill J, Fox A M, Lidzey D G, Oda M, Cabanillas-Gonzalez J and Bradley D D C 2003 Exciton migration in beta-phase poly(9,9-dioctylfluorene) *Phys. Rev.* B **67** 195333

[46] Korovyanko O J and Vardeny Z V 2002 Film morphology and ultrafast photoexcitation dynamics in polyfluorene *Chem. Phys. Lett.* **356** 361–7

[47] Basko D M, La Rocca G C, Bassani F and Agranovich V M 2005 Interaction of quantum well excitons with a resonant localized excitation *Phys. Rev.* B **71** 165330

[48] Lidzey D G, Bradley D D C, Armitage A, Walker S and Skolnick M S 2000 Photon-mediated hybridization of Frenkel excitons in organic semiconductor microcavities *Science* **288** 1620–3